Targeting microRNA-132 protects against kidney fibrosis and restricts myofibroblast differentiation from cells of renin lineage

Pluijm, L.A.K. van der; Koudijs, A.; Duijs, J.M.G.J.; Stam, W.; Rotmans, J.I.; Zonneveld, A.J. van; Bijkerk, R.

AMERICAN JOURNAL OF PHYSIOLOGY
CELL PHYSIOLOGY

Am J Physiol Cell Physiol 329: C1429–C1438, 2025.
First published September 27, 2025; doi:10.1152/ajpcell.00427.2025

RESEARCH ARTICLE

Exploring the Multifaceted Roles of Non-Coding RNAs in Human Diseases

Targeting microRNA-132 protects against kidney fibrosis and restricts myofibroblast differentiation from cells of renin lineage

Loïs A. K. van der Pluijm, Angela Koudijs, Jacques M. G. J. Duijs, Wendy Stam, Joris I. Rotmans, Anton Jan van Zonneveld, and Roel Bijkerk

Department of Internal Medicine (Nephrology) and the Einthoven Laboratory for Vascular and Regenerative Medicine, Leiden University Medical Centre, Leiden, The Netherlands

Abstract

Kidney fibrosis represents a central pathophysiological process in the progression of chronic kidney disease to end-stage kidney failure, yet its underlying cellular mechanisms remain incompletely understood. Cells of renin lineage (CoRL) have not only been shown to possess regenerative capacity following injury but may also contribute to fibrotic remodeling. MicroRNA-132 (miR-132), known to regulate both fibrotic signaling and renin synthesis, represents a potential therapeutic target to halt progression of kidney fibrosis. Here, we investigated the role of miR-132 and CoRL in two complementary models of kidney injury—5/6 nephrectomy and bilateral ischemia-reperfusion injury—using renin lineage-tracing mice treated with a miR-132 antimiR or scrambled control. In both models, miR-132 silencing improved renal function and led to a consistent reduction in interstitial fibrosis and myofibroblast accumulation in the kidney. The number of proliferating myofibroblasts also declined, supporting an antiproliferative effect. Podocyte number per glomerulus was significantly higher upon miR-132 silencing, indicating protection from glomerular damage. CoRL-derived podocytes were present in both models, but not affected by miR-132 knockdown, suggesting that the observed podocyte protection primarily results from reduced loss of resident cells. Lineage tracing further confirmed that CoRL contribute directly to the pool of α-smooth muscle actin + myofibroblasts. Interestingly, miR-132 silencing reduced the number of CoRL-derived myofibroblasts. Together, these findings identify miR-132 as a regulator of fibrotic remodeling and highlight the dual regenerative and fibrogenic potential of CoRL. Pharmacological inhibition of miR-132 may offer a promising approach to preserve kidney function and limiting fibrosis.

NEW & NOTEWORTHY This study demonstrates that cells of renin lineage (CoRL) directly contribute to the myofibroblast pool in two distinct models of kidney injury. Silencing of microRNA-132 reduces kidney fibrosis, preserves podocyte number, and attenuates myofibroblast proliferation, including those derived from CoRL. These findings highlight miR-132 as a promising target to curb fibrotic remodeling while preserving renal structure and uncover new insights into the dual regenerative and profibrotic plasticity of CoRL.

cells of renin lineage; kidney fibrosis; microRNA-132; myofibroblasts; podocyte preservation

INTRODUCTION

Kidney fibrosis is a hallmark of progressive kidney disease and a major contributor to the progression from acute kidney injury (AKI) to chronic kidney disease (CKD). It reflects a maladaptive repair response that ultimately leads to nephron loss and declining kidney function. Although current treatments may slow down disease progression, they do not directly target the underlying fibrotic mechanism (1, 2).

MicroRNAs (miRNAs) are small non-coding RNAs that regulate gene expression by repressing translation or promoting mRNA degradation. They have emerged as promising targets due to their ability to modulate entire gene networks (3). Among them, microRNA-132 (miR-132) has been implicated in fibrotic remodeling and organ dysfunction across multiple organs, including heart (4), lung (5), and liver (6). Notably, miR-132 antimiRs have already progressed into clinical trials for heart failure, highlighting their translational potential (7). Given its broad tissue distribution, including in the kidney, miR-132 modulation may also hold promise for renal disease. Supporting this notion, sequencing studies have shown that miR-132 is upregulated following ischemic kidney injury in experimental models (8).

We previously demonstrated that miR-132 silencing reduced myofibroblast accumulation in the unilateral

Correspondence: L. A. K. van der Pluijm (l.a.k.van_der_pluijm@lumc.nl); R. Bijkerk (r.bijkerk@lumc.nl).
Submitted 27 May 2025 / Revised 16 June 2025 / Accepted 12 September 2025

ureteral obstruction (UUO) model, yielding antifibrotic effects in the kidney as well (9). However, opposing results were obtained in a sepsis-induced ischemia-reperfusion injury (IRI) model, as protective effects of miR-132 overexpression on kidney fibrosis were reported (10). Together, these observations highlight the complex role of miR-132 in renal pathophysiology and point to the need for further studies in models that capture both structural and functional aspects of the clinical spectrum of kidney injury, enabling evaluation of miR-132 as a therapeutic target.

In parallel, increasing attention has turned to the cells of renin lineage (CoRL), a perivascular cell population traditionally known for their role in endocrine regulation of blood pressure via renin secretion. CoRL have been shown to possess remarkable plasticity following kidney injury, undergoing adaptive changes seemingly aiming to restore homeostasis by differentiating toward various cell types (11). Previous studies demonstrated that CoRL can contribute to the regeneration of podocytes (12) and erythropoietin (EPO)-producing cells (13) and may transiently adopt mesangial- (14) or pericyte (15)-like phenotypes to counteract vascular rarefaction. Given the established role of pericytes as a main source of myofibroblast during fibrogenesis (16), the possibility that CoRL themselves may give rise to myofibroblasts has become an important area of investigation. Although such a transition has been observed in a severe model of obstructive nephropathy (UUO) (17), its relevance in more progressive and clinically representative models of kidney disease that allow for renal function measurements remains unclear (18).

Adding to this complexity, emerging evidence suggests that miR-132 regulates the excretion of renin by CoRL (19). This raises the intriguing possibility that miR-132 not only influences fibrogenic signaling pathways but also modulates the plasticity and fate of CoRL following injury. To address this, we investigated the role of miR-132 and CoRL in two complementary models of renal injury—5/6 nephrectomy (5/6NX) and bilateral ischemia-reperfusion injury (bIRI)—which capture distinct aspects of kidney disease progression. Using renin lineage-trace mice (20), we assessed whether targeting miR-132 could preserve renal structure and function and dissect how CoRL contribute to repair versus fibrosis across these settings.

MATERIALS AND METHODS

Animals

Male C57BL/6J Ren1cre × Rs-tdTomato-R (JAX; The Jackson Laboratory) mice aged 9–12 wk were used in all experiments (healthy controls: $n = 5$; 5/6NX: scrambled, $n = 5$ and antimiR-132, $n = 8$; and bIRI: scrambled, $n = 8$ and antimiR-132, $n = 7$). Mice were housed under standard conditions with controlled temperature (20–22°C), humidity (55%), and a 12-h light/dark cycle. Food and water were provided ad libitum. All procedures were conducted in accordance with Dutch legislation (Experiments on Animals Act, Wod, 2014 revision) and EU directive 2010/63/EU, with approval from the Ethical Committee on Animal Care and Experimentation of Leiden University Medical Center (Permit No. AVD1160020171145).

Bilateral ischemia-reperfusion (bIRI) was induced, as previously described (21). Mice were temperature-regulated using a rectal probe. Using a dorsal incision approach, renal arteries and veins were clamped for 22 min. Clamps were then removed to allow reperfusion, confirming proper reflow by color change of the kidney. Mice were killed after 14 days by exsanguination.

For 5/6 nephrectomy (5/6NX), a two-step surgical procedure was performed. First, the left kidney was completely removed via a flank incision. After 7 days, the right kidney was exposed and its upper and lower poles were surgically excised and covered with styptic gelatin sponge. Fourteen days after the second surgery, mice were killed by exsanguination.

All surgical procedures were performed under isoflurane anesthesia (0.25%–4%), and peri- and postoperative analgesia were provided via subcutaneous buprenorphine injections (0.1 mg/kg).

Treatment with MicroRNA-132 AntimiR

Twenty-four hours before surgery (second surgery in the case of 5/6NX), 20 mg/kg locked nucleic acid (LNA) targeting miR-132 or a scrambled control (Exiqon) was administered intraperitoneally.

Blood Urea and Plasma Creatinine Measurements

Blood samples were collected via tail vein punctures throughout the 2-wk study period. Urea concentrations in whole blood were determined using a Reflotron Plus system (Roche Diagnostics). Endpoint plasma was collected by centrifuging whole blood in K2 EDTA-buffered tubes, and creatinine levels were determined with an enzymatic assay (Cat. No. 80350; Crystal Chem).

MicroRNA Isolation and TaqMan

Total RNA was isolated from freshly frozen kidney tissue (bIRI) using TRIzol reagent (Thermo Fisher) in combination with bead-based homogenization or from paraffin-embedded kidney sections (5/6NX) using the RNeasy FFPE kit (Qiagen). Reverse transcription of microRNAs was performed using the TaqMan MicroRNA reverse transcription kit (Applied Biosystems), using 250 ng total RNA as input. Quantitative polymerase chain reaction (PCR) was performed with TaqMan Universal Master Mix II (no UNG) and assays specific for miR-132 (TaqMan MicroRNA Assay, ID: 000457), miR-29a (TaqMan MicroRNA Assay, ID: 002112), and miR-212 (TaqMan MicroRNA Assay ID: 000515). U6 small nuclear RNA (TaqMan Assay, ID: 001973) was used as an endogenous control for normalization.

For mRNA analysis, cDNA synthesis was performed using the GoScript Reverse Transcription System (Promega). Quantitative PCR was performed with iTaq Universal SYBR Green Supermix (Bio-Rad) and gene-specific primers for Acta2 (fw: CCCCTGAAGAGCATCGGACA, rv: TGGCGGGGACATTGAAGGT) and Col1a1 (fw: TGACTGGGAAGAGCCGGAAGAGT, rv: GTTCCGGGCTGATGTACCAGT) with GAPDH as a reference gene. Relative expression levels were calculated using the $2^{-\Delta\Delta Ct}$ method.

Histology and Immunohistochemistry Evaluation

Kidneys were fixed in 10% neutral buffered formalin for 2 h, overnight incubated in 70% ethanol, and subsequently embedded in paraffin and sectioned at 4 μm thickness.

Periodic acid-Schiff staining was performed by a 45-min incubation with Schiff's reagent (Sigma), followed by a nuclear counterstain with hematoxylin for 45 s. Picrosirius Red (PSR) staining for collagen I and III was established by a 30-min incubation in direct red/fast green solution (Sigma). Immunohistochemical staining was obtained by performing antigen retrieval and blocking, after which sections were stained for tdTomato (1:500, AB1140-Origene or 1:500, LS-C60076-Isbio) and/or α-smooth muscle actin (αSMA) (1:200, mab1420-R&D Diagnostics), Col1a1 (ab21286, 1:200, Abcam), ki67 (1:200, 550609-BD Bioscience), and WT1 (1:500, AB89901-Abcam) overnight at 4°C and subsequently incubated with corresponding Alexa-secondary antibodies raised in donkey (1:250) for 2 h at room temperature. Sections were imaged using a slide scanner microscope (3DHISTECH).

All slides were digitalized, and automated image analysis for positive staining was performed using signal threshold analysis in NIH FIJI software. Ki67 positive cells were manually counted in 15 field of view (20×) per section per animal. Mesangial area was measured running a macro in FIJI on exported 16-bit images of 50 glomeruli per section using the auto threshold function based on the ISODATA algorithm (22).

Colocalization analysis was performed by creating marker-specific masks in HistoQuant software (3DHISTECH) for one section per animal. Podocyte quantification was performed by manually counting positive cells in at least 50 glomeruli per section per animal.

Statistics

All data were analyzed using GraphPad Prism. $P < 0.05$ was considered as statistically significant. To assess overall differences in urea levels between groups over time, the area under the curve (AUC) was calculated for each individual animal. Group comparisons were performed using an unpaired Student's *t* test on the AUC values. All other normally distributed endpoint data were compared using an unpaired Student's *t* test or one-way ANOVA with Tukey's post hoc test.

RESULTS

MicroRNA-132 Knockdown Improves Kidney Function in 5/6NX and bIRI

To investigate the fate of CoRL during kidney disease progression, we used a lineage-tracing mouse model expressing a tdTomato reporter under the control of the Ren1c promotor. Mice were treated with either a locked nucleic acid (LNA) antimiR targeting miR-132 or a scrambled control and subjected to 5/6NX or bIRI surgeries, followed by a 14-day monitoring period (Fig. 1*A*). Injury in both models was associated with increased miR-132 expression compared with healthy control kidneys, confirming its induction during disease (Fig. 1*B*). Effective silencing of miR-132 in kidney tissue was confirmed by quantitative reverse transcriptase polymerase chain reaction (qRT-PCR) (Fig. 1*B*).

To exclude nonspecific effects, we also quantified other fibrosis-related microRNAs. miR-29a, a well-known suppressor of extracellular matrix gene expression (23), was unchanged across groups in both models, indicating that its regulation is independent of miR-132 (APPENDIX Fig. A1*A*). miR-212, which is transcribed from the same locus and shares its seed sequence with miR-132 (24), showed a model-dependent response. In bIRI, miR-212 was elevated in scrambled animals but returned to near-control levels after antimiR-132 treatment, whereas in 5/6NX, it remained high in both groups (APPENDIX Fig. A1*B*). These data suggest that the observed effects on miR-212 are secondary and not the result of direct off-target silencing.

Kidney function, as measured by blood urea levels, significantly improved upon miR-132 knockdown in both models, indicating preserved kidney function compared with controls (Fig. 2*A*). In line with these findings, endpoint plasma creatinine levels were also significantly lower in antimiR-132-treated mice in both models (Fig. 2*B*). Body weight change over the 14-day study period did not differ significantly between treatment groups in either model.

Fibrotic Remodeling of the Kidney Is Attenuated by miR-132 Silencing

To explore the structural changes underlying this functional improvement, we next examined fibrotic remodeling. Picrosirius red (PSR) staining revealed a reduction in collagen I and III deposition following miR-132 silencing in both models, with ∼35% less PSR positive area in 5/6NX kidneys ($P < 0.01$) and around 20% reduction in bIRI kidneys ($P < 0.05$, Fig. 2, *C* and *D*).

To further characterize the antifibrotic effects of miR-132 knockdown, we evaluated α-smooth muscle actin (αSMA) expression as a marker of myofibroblast accumulation. As expected, both injury models exhibited robust αSMA+ interstitial populations. Importantly, treatment with the miR-132 inhibitor significantly reduced αSMA+ area—by ∼40% in 5/6NX ($P < 0.05$) and ∼30% in bIRI kidneys ($P < 0.01$)—indicating suppression of myofibroblast activation (Fig. 2, *E* and *H*).

To assess extracellular matrix production more specifically, we next examined collagen type I deposition using Col1a1 immunostaining, as type I collagen is a principal matrix component secreted by activated myofibroblasts (25). In line with the αSMA findings, miR-132 knockdown reduced Col1a1+ interstitial area by ∼33% in bIRI ($P < 0.05$), whereas no statistically significant difference was observed in 5/6NX ($P = 0.1$, Fig. 2, *F* and *I*). Histological observations were corroborated by qPCR analysis of Acta2 and Col1a1 expression in whole kidney RNA, which showed significantly lower transcript levels in bIRI and 5/6NX following miR-132 knockdown (APPENDIX Fig. A2).

MiR-132 Silencing Reduces Myofibroblast Proliferation

We next examined whether the reduction in myofibroblast abundance could be attributed to decreased proliferative activity. Costaining for αSMA and the proliferation marker *K*i-67 revealed that, in both models, a subset of αSMA+ cells

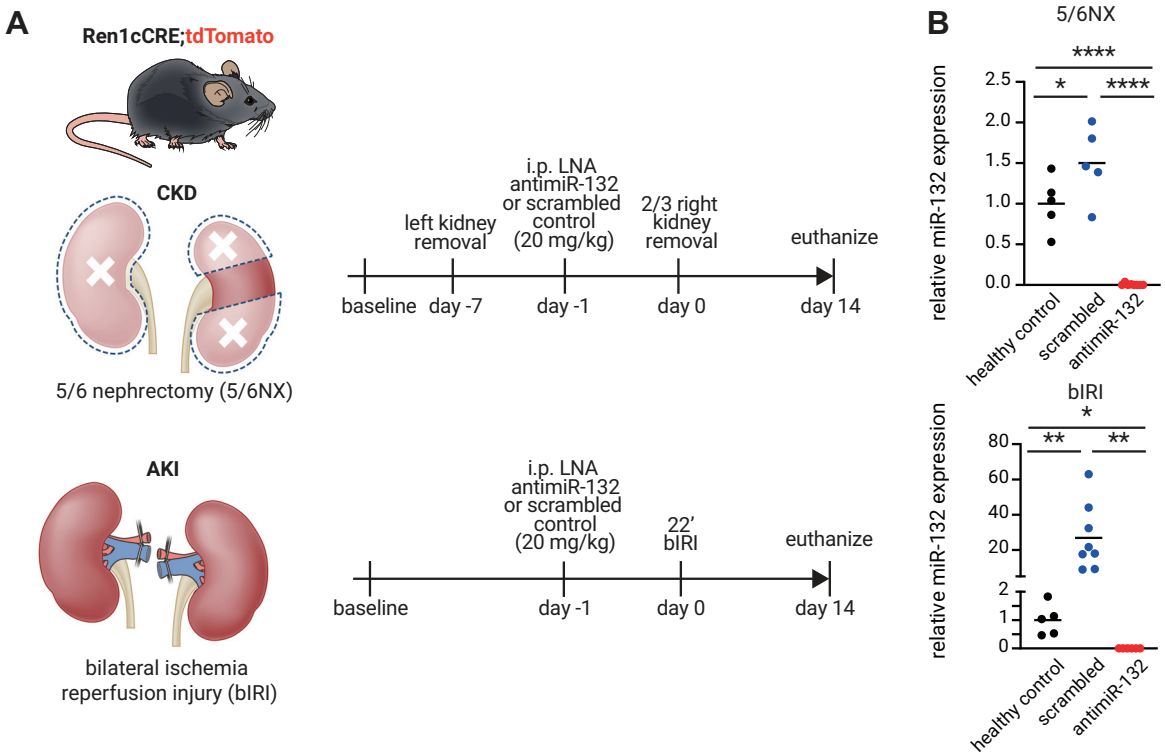

Figure 1. Experimental design and confirmation of renal miR-132 knockdown. *A*: schematic overview of the experimental workflow. Mice expressing tdTomato under the Ren1c promoter underwent either 5/6 nephrectomy (5/6NX) or bilateral ischemia-reperfusion injury (bIRI), and received one intraperitoneal (ip) injection of miR-132 antimiR or scrambled control. Mice were monitored for 14 days postinjury induction. *B*: quantitative RT-PCR analysis showing efficient knockdown of miR-132 in whole kidney tissue at endpoint (*day 14*). Data are presented as mean; each dot represents 1 animal ($n = 5$–8 per group). *$P < 0.05$; **$P < 0.01$, and ****$P < 0.0001$. Healthy controls are identical in both panels and are included as shared baseline in each model-specific ANOVA (5/6NX or bIRI), without statistical comparison between models. miR-132, microRNA-132.

was actively dividing (Fig. 2*G*). MiR-132 knockdown substantially lowered the number of αSMA+/Ki-67+ cells (Fig. 2*J*, $P < 0.05$), indicating reduced proliferation as a contributing factor in limiting myofibroblast expansion.

MiR-132 Silencing Prevents Podocyte Loss

Given that renal fibrosis can impact glomerular architecture, we next assessed glomerular size. MiR-132 inhibition led to an approximate 10% increase in glomerular area in bIRI ($P < 0.05$), whereas no different significant change was observed in 5/6NX ($P = 0.3$), possibly due to baseline glomerular hypertrophy inherent to the 5/6NX model (Fig. 2, *K* and *L*). Although glomerular enlargement may reflect maladaptive structural remodeling in some contexts, we did not observe associated mesangial expansion in either models (APPENDIX Fig. A3).

To further assess the glomerular integrity, we quantified podocyte number using WT1 immunostaining. MiR-132 knockdown increased the number of WT1+ cells per glomerulus in both models—from 8.5 to 9.9 in 5/6NX ($P < 0.05$) and from 9.0 to 11.0 in bIRI ($P < 0.01$)—indicating a consistent protective effect on this key epithelial cell type (Fig. 2, *M* and *N*).

MiR-132 Knockdown Does Not Markedly Alter CoRL-to-Podocyte Differentiation

In previous studies, we have shown that podocytes can be replenished from cells of renin lineage (CoRL) following kidney injury in both 5/6NX and bIRI (26). Next, we assessed whether the increase in podocyte number upon miR-132 silencing could be attributed to enhanced CoRL-to-podocyte differentiation. Costaining for tdTomato (CoRL) and WT1 confirmed the presence of CoRL-derived podocytes in both models (Fig. 3*A*). The number of CoRL-derived podocytes per glomerulus was comparable between groups, with an average difference of <1 cell per glomerulus, which did not reach significance ($P = 0.2$, Fig. 3*B*).

These findings imply that changes in lineage conversion are unlikely to account for the overall increase in podocyte number upon miR-132 knockdown, which is more likely attributable to reduced loss of resident podocytes.

MiR-132 Silencing Reduces CoRL-Derived Myofibroblasts

Given their pericyte-like properties, CoRL have been proposed to contribute to the myofibroblast population in kidney fibrosis (17). To further explore this hypothesis, we performed colocalization analysis of tdTomato+ cells (CoRL lineage) with αSMA, a marker of activated myofibroblasts. In both 5/6NX and bIRI kidneys, tdTomato+/αSMA+ double-positive cells were detected in the interstitium, confirming that a subset of myofibroblasts originates from CoRL (Fig. 3*C*).

Although their relative contribution to the overall αSMA+ population remained stable, the absolute area of CoRL-derived myofibroblasts was significantly reduced by ∼45% in 5/6NX and ∼40% in bIRI ($P < 0.05$, Fig. 3*D*) upon miR-132 knockdown. These findings confirm that CoRL actively

participate in fibrotic remodeling and that they integrate functionally into the myofibroblast pool during fibrosis, rather than forming a distinct or treatment-resistant subset.

DISCUSSION

This study extends current knowledge on the role of miR-132 in kidney fibrosis by validating its fibrotic effect in two

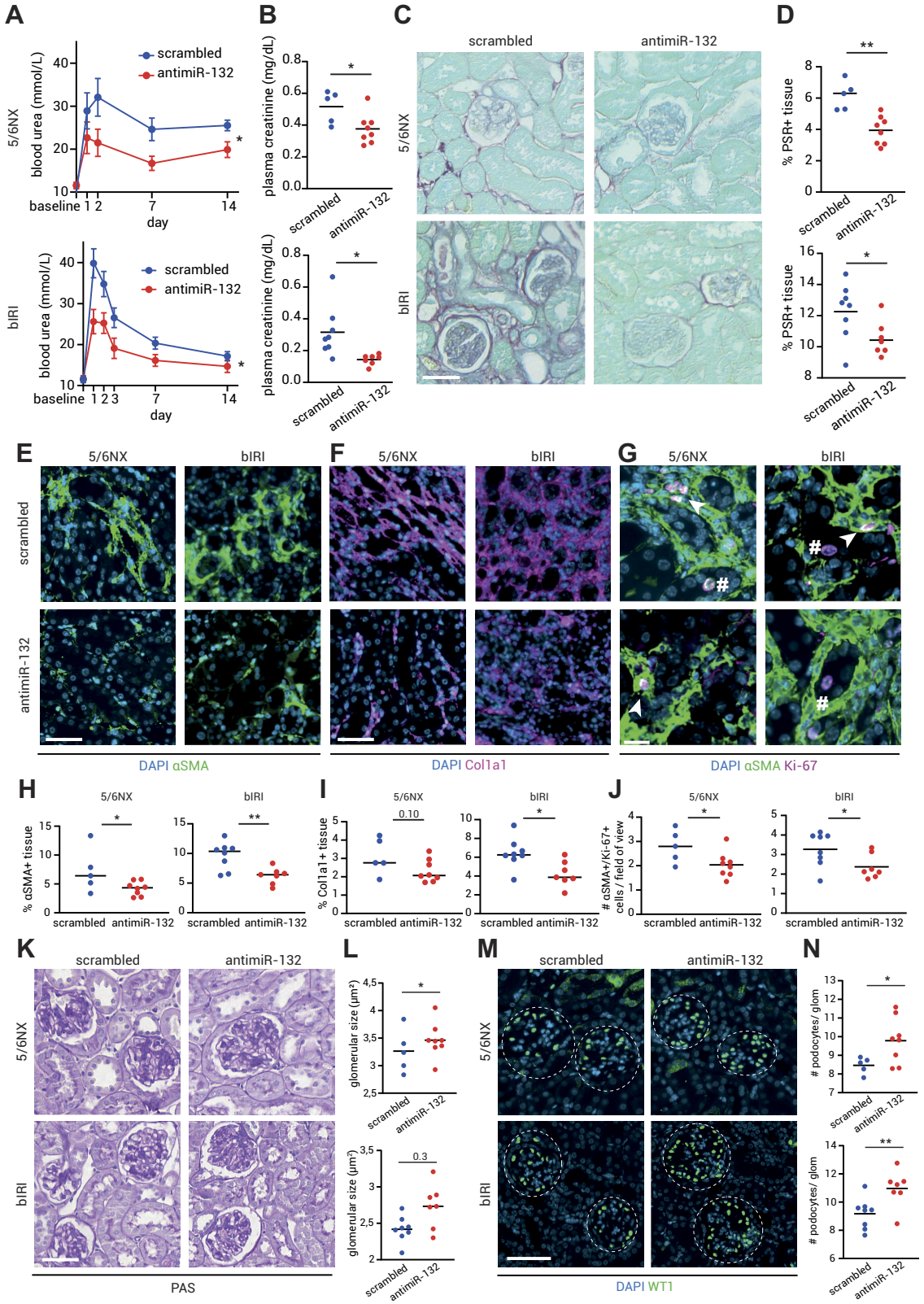

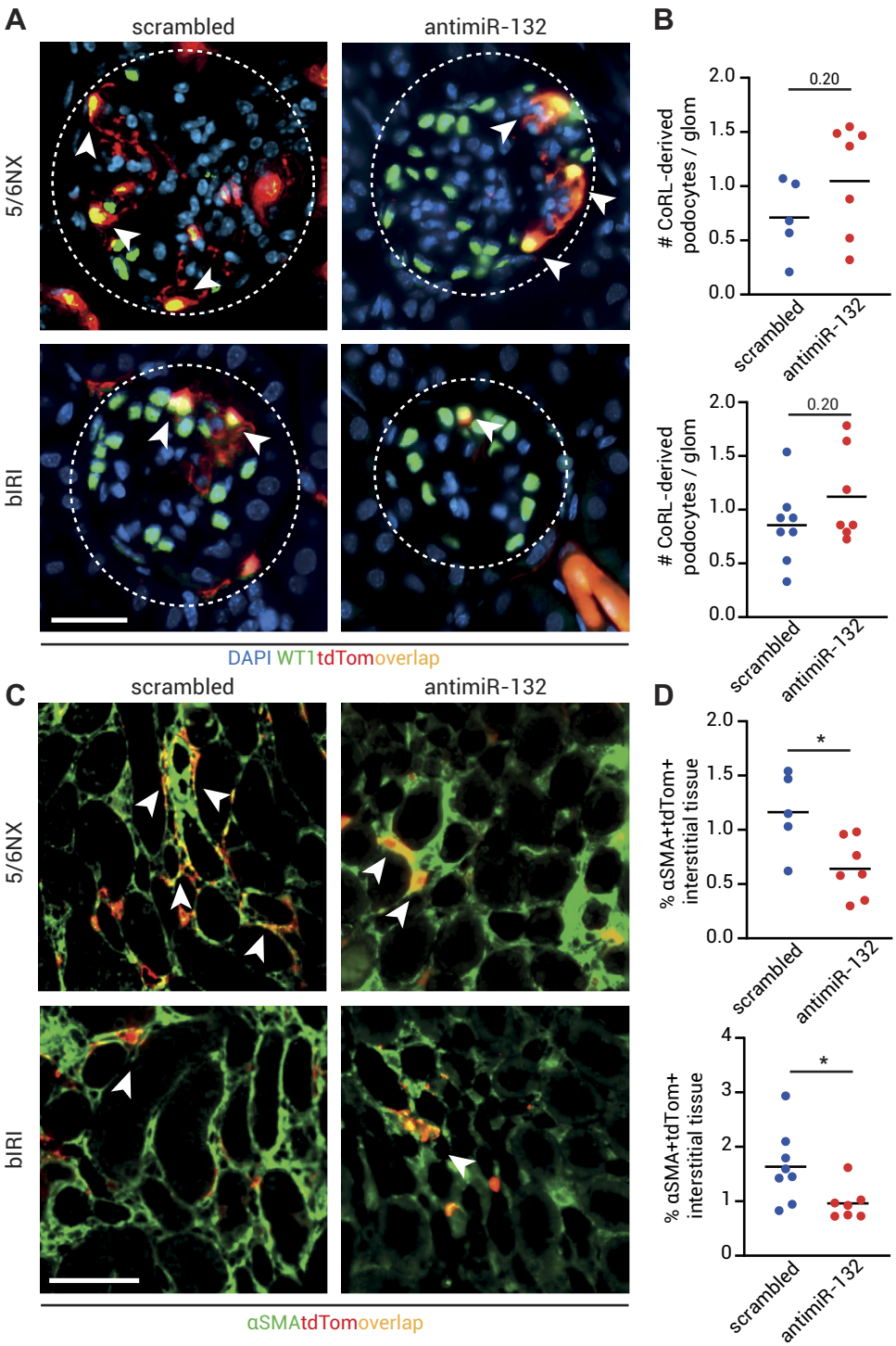

Figure 3. CoRL contribute to podocyte and myofibroblast populations in kidney injury, but their fate is not altered by miR-132 knockdown. *A*: representative images of glomerular costaining for tdTomato (CoRL, red) and WT1 (podocytes, green). Arrowheads indicate coexpression, suggesting podocytes derived from CoRL (yellow). Dotted lines indicate glomeruli, scale bar = 50 μm. *B*: quantification of tdTomato+/WT1+ double-positive cells per glomerulus in 5/6NX and bIRI, with or without miR-132 silencing. *C*: representative images of interstitial co-staining for tdTomato (CoRL, red) and αSMA (myofibroblasts, green). Arrowheads indicate coexpression, suggesting myofibroblasts derived from CoRL (yellow). Scale bar = 100 μm. *D*: quantification of tdTomato+/αSMA+ double-positive area. Data are presented as mean; each dot represents 1 animal (n = 5–8 per group). *$P < 0.05$. αSMA, α-smooth muscle actin; 5/6NX, 5/6 nephrectomy; bIRI, bilateral ischemia-reperfusion injury; CoRL, cells of renin lineage; miR-132, microRNA-132.

Figure 2. MiR-132 inhibition preserves kidney function by limiting fibrosis and podocyte loss. Blood urea (*A*) and plasma creatinine (*B*) levels following 5/6NX or bIRI show improved kidney function in miR-132-silenced mice compared with scrambled controls. *C*: representative Picro Sirius Red (PSR) staining of kidney sections. *D*: quantification of PSR-positive area. *E*: representative αSMA immunostaining showing interstitial myofibroblasts (green). *F*: representative Col1a1 staining (purple). *G*: representative images of costaining for αSMA and Ki-67 in the kidney medulla. Arrow heads point at examples of double positive cells, whereas hashtags mark examples of other proliferative (tubular) cells. *H–J*: quantification of αSMA+, Col1a1+, Ki-67+ cells, respectively. *K*: Periodic acid-Schiff (PAS) staining of the renal cortex with glomeruli. *L*: quantification of glomerular cross-sectional area. *M*: WT1 immunostaining of podocytes. *N*: quantification of WT1+ cells per glomerulus. Dotted lines indicate glomeruli. Scalebar = 100 μm. Data are presented as mean; each dot represents 1 animal (n = 5–8 per group); statistical significance for blood urea was calculated on the individual AUC values (unpaired Student's t test). *$P < 0.05$ and **$P < 0.01$. αSMA, α-smooth muscle actin; 5/6NX, 5/6 nephrectomy; AUC, area under the curve; bIRI, bilateral ischemia-reperfusion injury; miR-132, microRNA-132.

complementary mouse models—5/6 nephrectomy (5/6NX) and bilateral ischemia-reperfusion injury (bIRI). We demonstrate that miR-132 knockdown consistently reduces interstitial fibrosis, suppresses myofibroblast accumulation and proliferation, and preserves podocyte number. These effects across models suggest that miR-132 broadly affects fibrogenic processes and support its potential as a therapeutic target in chronic kidney disease. In addition, by using renin lineage tracing, we show that a subset of fibrogenic cells arises from cells of renin lineage (CoRL), highlighting their active participation in fibrotic remodeling and their responsiveness to miR-132 silencing.

MiR-132 knockdown exerted antifibrotic effects that were apparent in both tissue remodeling and myofibroblast behavior. In both models, reduced αSMA expression and decreased collagen accumulation (assessed by PSR), combined with lower numbers of proliferating myofibroblasts, indicated that miR-132 modulates both activation and expansion of fibrogenic cells. These effects extend prior findings in the unilateral ureteral obstruction (UUO) model (9) and demonstrate that miR-132 knockdown is also effective in settings that more closely resemble progressive human kidney disease (18). Although widely used, these models have their inherent limitations as well. For instance, bIRI is largely self-limiting and shows substantial functional recovery by *day 14*, which may mask long-term effects of intervention with antimiR-132. Yet, as the repertoire of injury models continues to expand to include both acute and progressive paradigms, converging results across systems increasingly support the robustness of miR-132's fibrotic effects.

Although the precise downstream targets of miR-132 in the kidney remain incompletely defined, prior work has linked it to TGF-β signaling and (myo)fibroblast proliferation without affecting tubular cell proliferation during repair, which we also confirmed in the 5/6NX and bIRI models. The same study identified FOXO3 and p300 as additional mediators of profibrotic transcription (9), but in our models we did not detect changes in these pathways or in TGF-β downstream targets Smad2/3 at whole kidney level, likely due to dilution of cell-specific effects in bulk RNA. Others have implicated Sirt1 as a key target, linking miR-132 to oxidative stress and tubular apoptosis (8). These findings suggest that miR-132 may act through multiple pathways protecting the kidney, depending on cell type and injury context.

Importantly, lineage tracing further revealed that a consistent fraction of αSMA+ myofibroblasts originates from CoRL, confirming earlier findings from others in the UUO model (17) and extending them to other kidney disease models with different injury dynamics. Although absolute numbers of CoRL-derived myofibroblasts declined following miR-132 knockdown, their relative contribution to the total myofibroblast pool remained stable. This indicates that CoRL-derived myofibroblasts respond to treatment similar to other fibrogenic cell types, further supporting their functional integration into the fibrotic niche. These findings reinforce the concept that CoRL are highly plastic and injury-responsive. While classically viewed as endocrine regulators, they can adopt mesenchymal phenotypes, including pericyte- and myofibroblast-like states. Although such transitions may initially serve regenerative or stabilizing roles, they become maladaptive when sustained. Our findings place CoRL within a broader group of perivascular stromal cells that exhibit similar plasticity: other subsets, such as Meflin-expressing fibroblasts, have likewise been shown to convert into myofibroblasts and modulate fibrosis through regulation of proliferation (27). Together with lineage-tracing and single-cell studies highlighting the heterogeneous origins of myofibroblasts, this underscores a shared capacity among mesenchymal populations to adopt profibrotic identities under stress, an insight that may guide future efforts to target fibrosis at its source (16, 28).

In addition to attenuating fibrosis, miR-132 knockdown also preserved glomerular architecture (in bIRI) and podocyte number in both kidney injury models. Given the central role of podocyte depletion in glomerulosclerosis and progression to end-stage kidney disease (29), this protective

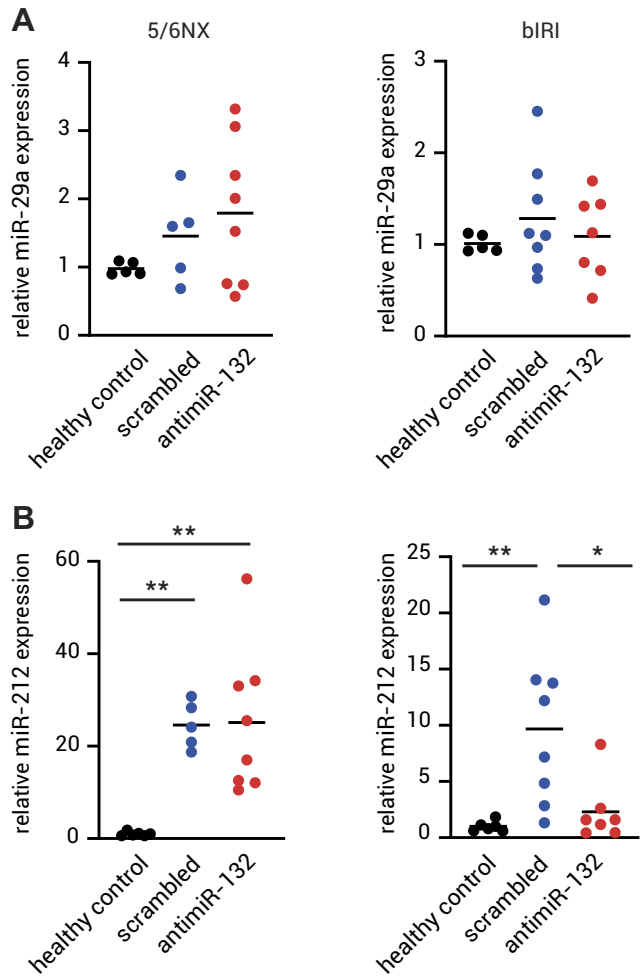

Figure A1. Expression of fibrosis-related microRNAs in kidney injury upon miR-132 knockdown. miR-29a (*A*) and miR-212 (*B*) expression in healthy controls, scrambled, and antimiR-132-treated groups in 5/6NX and bIRI models measured by qRT-PCR. Expression levels are normalized to U6 small nuclear RNA and presented relative to the mean of the healthy control group. Data are presented as mean; each dot represents 1 animal (n = 5–8 per group). Healthy controls are identical in both panels and are included as shared baseline in each model-specific ANOVA (5/6NX or bIRI), without statistical comparison between models. *$P < 0.05$ and **$P < 0.01$. 5/6NX, 5/6 nephrectomy; bIRI, bilateral ischemia-reperfusion injury; miR-132, microRNA-132; qRT-PCR, quantitative reverse transcriptase polymerase chain reaction.

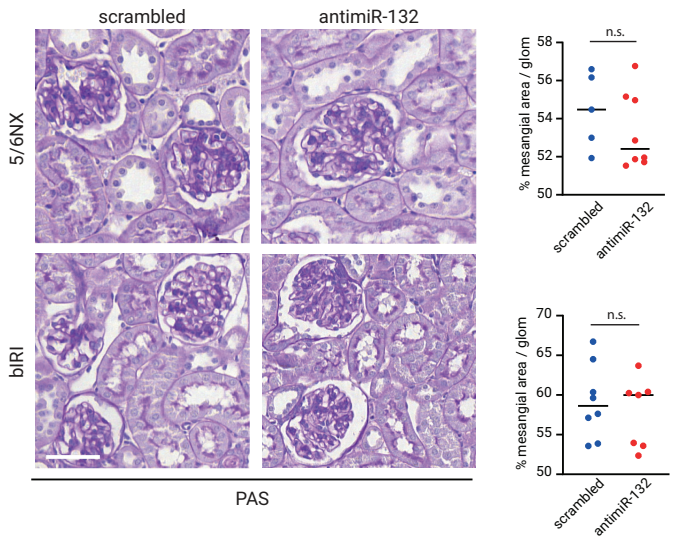

Figure A2. Mesangial area is not altered by miR-132 inhibition in 5/6NX and bIRI. Representative PAS images of 5/6NX and bIRI kidneys with and without miR-132 inhibitory treatment and corresponding quantification of percentage mesangial area per glomerulus. Scale bar = 100 µm. Data are presented as mean; each dot represents 1 animal (n = 5–8 per group). ns, P not significant. 5/6NX, 5/6 nephrectomy; bIRI, bilateral ischemia-reperfusion injury; glom, glomerulus; miR-132, microRNA-132; PAS, Periodic acid-Schiff.

effect likely contributes substantially to the improved kidney function observed. We used blood urea and creatinine levels as a readout of kidney function; however, more direct measurements such as glomerular filtration rate or albuminuria would be needed to fully capture changes in renal physiology. Notably, our lineage trace data as well as the postmitotic nature of resident podocytes (30) argue against increased proliferation or enhanced recruitment from CoRL as the underlying mechanism. Instead, miR-132 knockdown likely protects the existing podocytes from injury or loss, plausibly through reduced fibrotic remodeling and consequent stabilization of glomerular pressure dynamics (31). Interestingly, other studies have shown that miR-132 upregulation can also stabilize podocyte structures in glomerulosclerosis (32), suggesting that its effects are highly context-dependent. This apparent contrast highlights the complex interplay between microRNAs, signaling pathways, and cellular environment, where small shifts in expression or timing may significantly alter outcomes.

Although systemic miR-132 inhibition yielded clear renal benefits, it also raises questions about tissue specificity and broader physiological impact. To explore potential off-target effects, we quantified other fibrosis-related microRNAs. MiR-29a, a potent inhibitor of collagen and extracellular matrix gene expression (23), was unchanged in both models. By contrast, miR-212, which shares an identical seed sequence with miR132 as part of the miR-132/212 cluster (24), was reduced to control levels in bIRI upon miR-132 knockdown, but remained elevated in 5/6NX. Given the >5 nucleotide differences outside the seed, direct binding by the single-miRNA LNA inhibitor is unlikely. Similar context-dependent effects have been reported, with antimiR-132 reducing miR-212 in liver fibrosis (6), but not in the hippocampus (33), supporting an indirect mechanism via reduced injury-driven transcription of the miR-132/212 cluster. Also other miRNAs, for example, canonical miRNAs such as miR-21 (34) and miR-34 (35), have well-documented roles in renal fibrosis and could provide alternative targeting options. Nonetheless, our data points to a distinct role for miR-132 in myofibroblast-associated pathways.

The specific antimiR used in this study was administered systemically without cell type-specific targeting, limiting our ability to distinguish direct from indirect effects. Although no overt adverse effects were observed, miR-132 has known functions in other tissues, including the nervous (36), immune (37), and vascular (38) systems. Future studies using conditional knockouts targeting myofibroblasts, CoRL, or other specific cell types, will be crucial to dissect cell type-specific effects and minimize off-target consequences. Such precision may ultimately be necessary to safely translate miR-132-based therapies into clinical interventions.

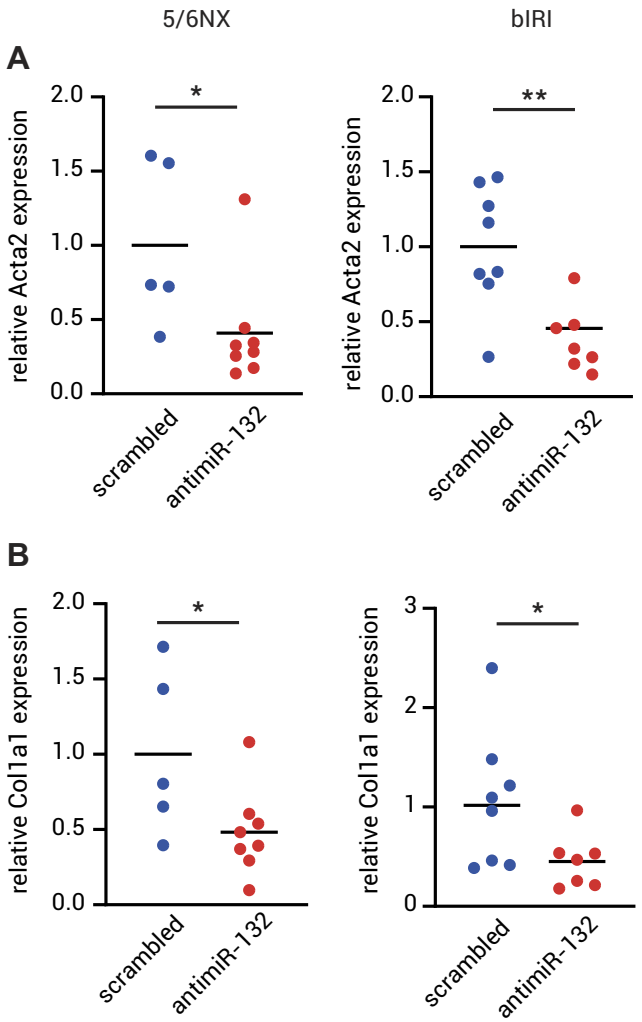

Figure A3. Quantitative PCR analysis of Acta2 and Col1a1 expression in kidney tissue from 5/6NX and bIRI. Relative gene expression levels of Acta2 (*A*) and Col1a1 (*B*) in 5/6NX and bIRI with and without miR-132 knockdown. Expression levels were normalized against GAPDH. In both models, Acta2 and Col1a1 expression were significantly reduced upon miR-132 knockdown, in line with histological findings (Fig. 2). Data are presented as mean; each dot represents 1 animal (n = 5–8 per group). *P < 0.05 and **P < 0.01. 5/6NX, 5/6 nephrectomy; bIRI, bilateral ischemia-reperfusion injury; miR-132, microRNA-132; PCR, polymerase chain reaction.

In summary, our findings establish miR-132 as a key regulator of kidney injury response, with effects in both fibrotic remodeling and podocyte preservation. We show that CoRL contribute directly to the myofibroblast pool in progressive disease models and respond to miR-132 knockdown in a manner consistent with their adopted fibrotic fate. Together, these data support the therapeutic potential of miR-132 silencing to limit fibrosis while preserving essential glomerular structures. Future studies leveraging spatial or single-cell transcriptomic approaches will be instrumental in identifying the molecular switches that govern CoRL plasticity and determining how to guide their fate toward regeneration rather than fibrosis.

APPENDIX

Additional data supporting the main findings are provided in the Appendix. Expression of other fibrosis-related microRNAs is shown in Appendix Fig. A1. Analysis of Acta2 and Col1a1 mRNA levels in kidney tissue from both injury models is presented in Appendix Fig. A2. Assessment of mesangial expansion is provided in Appendix Fig. A3.

DATA AVAILABILITY

Data will be made available upon reasonable request.

ACKNOWLEDGMENTS

The mouse strain in this study was created with the support of the Roswell Park Comprehensive Cancer and National Cancer Institute (NCI) Grant P30CAO16056 and was kindly provided by Prof. Kenneth W. Gross. Visual abstract by M.S. Zuurmond.

GRANTS

This work was funded by the Dutch Kidney Foundation (20OK015) and EFSD/Novo Nordisk Foundation Future Leaders Award Program (NNF23SA0087433).

DISCLOSURES

No conflicts of interest, financial or otherwise, are declared by the authors.

AUTHOR CONTRIBUTIONS

L.A.K.v.d.P. and R.B. conceived and designed research; L.A.K.v.d.P., A.K., J.M.G.J.D., and W.S. performed experiments; L.A.K.v.d.P. and R.B. analyzed data; L.A.K.v.d.P. and R.B. interpreted results of experiments; L.A.K.v.d.P. prepared figures; L.A.K.v.d.P. drafted manuscript; A.K., W.S., J.I.R., A.J.v.Z., and R.B. edited and revised manuscript; L.A.K.v.d.P. and R.B. approved final version of manuscript.

REFERENCES

1. **Zhang T**, **Widdop RE**, **Ricardo SD.** Transition from acute kidney injury to chronic kidney disease: mechanisms, models, and biomarkers. *Am J Physiol Renal Physiol* 327: F788–F805, 2024. doi:10.1152/ajprenal.00184.2024.
2. **Hewitson TD.** Renal tubulointerstitial fibrosis: common but never simple. *Am J Physiol Renal Physiol* 296: F1239–F1244, 2009. doi:10.1152/ajprenal.90521.2008.
3. **Rani V**, **Sengar RS.** Biogenesis and mechanisms of microRNA-mediated gene regulation. *Biotechnol Bioeng* 119: 685–692, 2022. doi:10.1002/bit.28029.
4. **Wang G**, **Wang R**, **Ruan Z**, **Liu L**, **Li Y**, **Zhu L.** MicroRNA-132 attenuated cardiac fibrosis in myocardial infarction-induced heart failure rats. *Biosci Rep* 40: BSR20201696, 2020. doi:10.1042/BSR20201696.
5. **Fang S**, **Wang T**, **Weng L**, **Han X**, **Zheng R**, **Zhang H.** Lung cancer-derived exosomal miR-132-3p contributed to interstitial lung disease development. *World J Surg Oncol* 21: 205, 2023. doi:10.1186/s12957-023-03095-6.
6. **Momen-Heravi F**, **Catalano D**, **Talis A**, **Szabo G**, **Bala S.** Protective effect of LNA-anti-miR-132 therapy on liver fibrosis in mice. *Mol Ther Nucleic Acids* 25: 155–167, 2021. doi:10.1016/j.omtn.2021.05.007.
7. **Täubel J**, **Hauke W**, **Rump S**, **Viereck J**, **Batkai S**, **Poetzsch J**, **Rode L**, **Weigt H**, **Genschel C**, **Lorch U**, **Theek C**, **Levin AA**, **Bauersachs J**, **Solomon SD**, **Thum T.** Novel antisense therapy targeting microRNA-132 in patients with heart failure: results of a first-in-human phase 1b randomized, double-blind, placebo-controlled study. *Eur Heart J* 42: 178–188, 2021. doi:10.1093/eurheartj/ehaa898.
8. **Li C**, **Han S**, **Zhu J**, **Cheng F.** MiR-132-3p activation aggravates renal ischemia-reperfusion injury by targeting Sirt1/PGC1alpha axis. *Cell Signal* 110: 110801, 2023. doi:10.1016/j.cellsig.2023.110801.
9. **Bijkerk R**, **de Bruin RG**, **van Solingen C**, **van Gils JM**, **Duijs JMGJ**, **van der Veer EP**, **Rabelink TJ**, **Humphreys BD**, **van Zonneveld AJ.** Silencing of microRNA-132 reduces renal fibrosis by selectively inhibiting myofibroblast proliferation. *Kidney Int* 89: 1268–1280, 2016. doi:10.1016/j.kint.2016.01.029.
10. **Zhang D**, **Lu H**, **Hou W**, **Bai Y**, **Wu X.** Effect of miR-132-3p on sepsis-induced acute kidney injury in mice via regulating HAVCR1/KIM-1. *Am J Transl Res* 13: 7794–7803, 2021.
11. **Broeker KAE**, **Schrankl J**, **Fuchs MAA**, **Kurtz A.** Flexible and multifaceted: the plasticity of renin-expressing cells. *Pflugers Arch* 474: 799–812, 2022. doi:10.1007/s00424-022-02694-8.
12. **Pippin JW**, **Sparks MA**, **Glenn ST**, **Buitrago S**, **Coffman TM**, **Duffield JS**, **Gross KW**, **Shankland SJ.** Cells of renin lineage are progenitors of podocytes and parietal epithelial cells in experimental glomerular disease. *Am J Pathol* 183: 542–557, 2013. doi:10.1016/j.ajpath.2013.04.024.
13. **Broeker KAE**, **Fuchs MAA**, **Schrankl J**, **Lehrmann C**, **Schley G**, **Todorov VT**, **Hugo C**, **Wagner C**, **Kurtz A.** Prolyl-4-hydroxylases 2 and 3 control erythropoietin production in renin-expressing cells of mouse kidneys. *J Physiol* 600: 671–694, 2022. doi:10.1113/JP282615.
14. **Starke C**, **Betz H**, **Hickmann L**, **Lachmann P**, **Neubauer B**, **Kopp JB**, **Sequeira-Lopez MLS**, **Gomez RA**, **Hohenstein B**, **Todorov VT**, **Hugo CPM.** Renin lineage cells repopulate the glomerular mesangium after injury. *J Am Soc Nephrol* 26: 48–54, 2015. doi:10.1681/asn.2014030265.
15. **Pippin JW**, **Kaverina NV**, **Eng DG**, **Krofft RD**, **Glenn ST**, **Duffield JS**, **Gross KW**, **Shankland SJ.** Cells of renin lineage are adult pluripotent progenitors in experimental glomerular disease. *Am J Physiol Renal Physiol* 309: F341–F58, 2015. doi:10.1152/ajprenal.00438.2014.
16. **Humphreys BD**, **Lin SL**, **Kobayashi A**, **Hudson TE**, **Nowlin BT**, **Bonventre JV**, **Valerius MT**, **McMahon AP**, **Duffield JS.** Fate tracing reveals the pericyte and not epithelial origin of myofibroblasts in kidney fibrosis. *Am J Pathol* 176: 85–97, 2010. doi:10.2353/ajpath.2010.090517.
17. **Stefanska A**, **Eng D**, **Kaverina N**, **Pippin JW**, **Gross KW**, **Duffield JS**, **Shankland SJ.** Cells of renin lineage express hypoxia inducible factor 2α following experimental ureteral obstruction. *BMC Nephrol* 17: 5, 2016. doi:10.1186/s12882-015-0216-0.
18. **Eddy AA**, **López-Guisa JM**, **Okamura DM**, **Yamaguchi I.** Investigating mechanisms of chronic kidney disease in mouse models. *Pediatr Nephrol* 27: 1233–1247, 2012. doi:10.1007/s00467-011-1938-2.
19. **van Zonneveld AJ**, **Au YW**, **Stam W**, **van Gelderen S**, **Rotmans JI**, **Deen PMT**, **Rabelink TJ**, **Bijkerk R.** MicroRNA-132 regulates salt-dependent steady-state renin levels in mice. *Commun Biol* 3: 238, 2020. doi:10.1038/s42003-020-0967-4.
20. **Glenn ST.** *Generation of Renin BAC Transgenic Models for the Study of Regulation, Lineage Tracing, and Tumorigenic Potential of the Renin-Expressing Cell* (*Dissertation*). Buffalo, New York: State University of New York, 2014.

21. **Wei Q**, **Dong Z.** Mouse model of ischemic acute kidney injury: technical notes and tricks. *Am J Physiol Renal Physiol* 303: F1487–F1494, 2012. doi:10.1152/ajprenal.00352.2012.
22. **Ridler TW**, **Calvard S.** Picture thresholding using an iterative selection method. *IEEE Trans Syst Man Cybern* 8: 630–632, 1978. doi:10.1109/TSMC.1978.4310039.
23. **Wang B**, **Wang J**, **He W**, **Zhao Y**, **Zhang A**, **Liu Y**, **Hassounah F**, **Ma F**, **Klein JD**, **Wang XH**, **Wang H.** Exogenous miR-29a attenuates muscle atrophy and kidney fibrosis in unilateral ureteral obstruction mice. *Hum Gene Ther* 31: 367–375, 2020. doi:10.1089/hum.2019.287.
24. **Ucar A**, **Vafaizadeh V**, **Jarry H**, **Fiedler J**, **Klemmt PAB**, **Thum T**, **Groner B**, **Chowdhury K.** miR-212 and miR-132 are required for epithelial stromal interactions necessary for mouse mammary gland development. *Nat Genet* 42: 1101–1108, 2010. doi:10.1038/ng.709.
25. **Nakagawa N**, **Duffield JS.** Myofibroblasts in fibrotic kidneys. *Curr Pathobiol Rep* 1: 10.1007/s40139-013-0025-8, 2013. doi:10.1007/s40139-013-0025-8.
26. **van der Pluijm LAK**, **Koudijs A**, **Stam W**, **Roelofs JJTH**, **Danser AHJ**, **Rotmans JI**, **Gross KW**, **Pieper MP**, **van Zonneveld AJ**, **Bijkerk R.** SGLT2 inhibition promotes glomerular repopulation by cells of renin lineage in experimental kidney disease. *Acta Physiol (Oxf)* 240: e14108, 2024. doi:10.1111/apha.14108.
27. **Minatoguchi S**, **Saito S**, **Furuhashi K**, **Sawa Y**, **Okazaki M**, **Shimamura Y**, **Kaihan AB**, **Hashimoto Y**, **Yasuda Y**, **Hara A**, **Mizutani Y**, **Ando R**, **Kato N**, **Ishimoto T**, **Tsuboi N**, **Esaki N**, **Matsuyama M**, **Shiraki Y**, **Kobayashi H**, **Asai N**, **Enomoto A**, **Maruyama S.** A novel renal perivascular mesenchymal cell subset gives rise to fibroblasts distinct from classic myofibroblasts. *Sci Rep* 12: 5389, 2022. doi:10.1038/s41598-022-09331-5.
28. **Falke LL**, **Gholizadeh S**, **Goldschmeding R**, **Kok RJ**, **Nguyen TQ.** Diverse origins of the myofibroblast—implications for kidney fibrosis. *Nat Rev Nephrol* 11: 233–244, 2015. doi:10.1038/nrneph.2014.246.
29. **Kriz W.** Podocyte is the major culprit accounting for the progression of chronic renal disease. *Microsc Res Tech* 57: 189–195, 2002. doi:10.1002/jemt.10072.
30. **Lasagni L**, **Lazzeri E**, **Shankland SJ**, **Anders HJ**, **Romagnani P.** Podocyte mitosis - a catastrophe. *Curr Mol Med* 13: 13–23, 2013. doi:10.2174/1566524011307010013.
31. **Lopes TG**, **de Souza ML**, **da Silva VD**, **Dos Santos M**, **da Silva WIC**, **Itaquy TP**, **Garbin HI**, **Veronese FV.** Markers of renal fibrosis: how do they correlate with podocyte damage in glomerular diseases? *PLoS One* 14: e0217585, 2019. doi:10.1371/journal.pone.0217585.
32. **Li M**, **Armelloni S**, **Zennaro C**, **Wei C**, **Corbelli A**, **Ikehata M**, **Berra S**, **Giardino L**, **Mattinzoli D**, **Watanabe S**, **Agostoni C**, **Edefonti A**, **Reiser J**, **Messa P**, **Rastaldi MP.** BDNF repairs podocyte damage by microRNA-mediated increase of actin polymerization. *J Pathol* 235: 731–744, 2015. doi:10.1002/path.4484.
33. **Walgrave H**, **Penning A**, **Tosoni G**, **Snoeck S**, **Davie K**, **Davis E**, **Wolfs L**, **Sierksma A**, **Mars M**, **Bu T**, **Thrupp N**, **Zhou L**, **Moechars D**, **Mancuso R**, **Fiers M**, **Howden AJM**, **De Strooper B**, **Salta E.** microRNA-132 regulates gene expression programs involved in microglial homeostasis. *iScience* 26: 106829, 2023. doi:10.1016/j.isci.2023.106829.
34. **Chau BN**, **Xin C**, **Hartner J**, **Ren S**, **Castano AP**, **Linn G**, **Li J**, **Tran PT**, **Kaimal V**, **Huang X**, **Chang AN**, **Li S**, **Kalra A**, **Grafals M**, **Portilla D**, **MacKenna DA**, **Orkin SH**, **Duffield JS.** MicroRNA-21 promotes fibrosis of the kidney by silencing metabolic pathways. *Sci Transl Med* 4: 121ra18, 2012. doi:10.1126/scitranslmed.3003205.
35. **Liu Y**, **Bi X**, **Xiong J**, **Han W**, **Xiao T**, **Xu X**, **Yang K**, **Liu C**, **Jiang W**, **He T**, **Yu Y**, **Li Y**, **Zhang J**, **Zhang B**, **Zhao J.** MicroRNA-34a promotes renal fibrosis by downregulation of klotho in tubular epithelial cells. *Mol Ther* 27: 1051–1065, 2019. doi:10.1016/j.ymthe.2019.02.009.
36. **Qian Y**, **Song J**, **Ouyang Y**, **Han Q**, **Chen W**, **Zhao X**, **Xie Y**, **Chen Y**, **Yuan W**, **Fan C.** Advances in roles of miR-132 in the nervous system. *Front Pharmacol* 8: 770, 2017. doi:10.3389/fphar.2017.00770.
37. **Shaked I**, **Meerson A**, **Wolf Y**, **Avni R**, **Greenberg D**, **Gilboa-Geffen A**, **Soreq H.** MicroRNA-132 potentiates cholinergic anti-inflammatory signaling by targeting acetylcholinesterase. *Immunity* 31: 965–973, 2009. doi:10.1016/j.immuni.2009.09.019.
38. **Anand S**, **Majeti BK**, **Acevedo LM**, **Murphy EA**, **Mukthavaram R**, **Scheppke L**, **Huang M**, **Shields DJ**, **Lindquist JN**, **Lapinski PE**, **King PD**, **Weis SM**, **Cheresh DA.** MicroRNA-132–mediated loss of p120RasGAP activates the endothelium to facilitate pathological angiogenesis. *Nat Med* 16: 909–914, 2010. doi:10.1038/nm.2186.